

**Synchronous emplacement of anorthosite xenoliths, the  
Beaver River diabase, and the Greenstone Flow**

**Yiming Zhang<sup>1</sup>, Nicholas L. Swanson-Hysell<sup>1</sup>, Mark D. Schmitz<sup>2</sup>, Margaret S.  
Avery<sup>1</sup>, James D. Miller Jr.<sup>3</sup>**

<sup>1</sup>Department of Earth and Planetary Science, University of California, Berkeley, CA, USA

<sup>2</sup>Department of Geosciences, Boise State University, Boise, ID, USA

<sup>3</sup>Department of Earth and Environmental Sciences, University of Minnesota, Duluth, MN, USA

**Key Points:**

- New geochronology data precisely constrain the timing of emplacement of large anorthosite xenoliths within the Beaver River diabase of the Midcontinent Rift.
- Paleomagnetic and geochronological data support that the Beaver River diabase is comagmatic with the very high volume Greenstone Flow.
- Wide conduits of magma towards the surface are indicated by >100 meter diameter anorthosite xenoliths.

---

Corresponding author: Yiming Zhang, [yimingzhang@berkeley.edu](mailto:yimingzhang@berkeley.edu)

15 **Abstract**

16 New geochronologic and paleomagnetic data from the North American Midcontinent Rift  
 17 reveal the synchronous emplacement of the Beaver River diabase, the anorthosite xenoliths within it, and the Greenstone Flow — one of the largest lava flows on Earth. A U-  
 18 Pb zircon date from one of the anorthosite xenoliths of  $1091.83 \pm 0.21$  Ma is consistent  
 19 with the anorthosite cumulate forming as part of the Midcontinent Rift although it could  
 20 have been reset by a long residence time within high-temperature tholeiitic magma. Re-  
 21 gardless, the date provides a maximum age constraint for the Beaver River diabase. Paired  
 22 with the minimum age constraint of a cross-cutting Silver Bay intrusion ( $1091.61 \pm 0.14$   
 23 Ma) these data tightly constrain the age of the Beaver River diabase to be coeval with  
 24 the eruption of the Portage Lake Volcanics — which is further supported by similar tilt-  
 25 corrected paleomagnetic pole positions. These data, as well as mineralogical and geo-  
 26 chemical data, support the hypothesis that the Beaver River diabase that entrained large  
 27 anorthosite xenoliths was the feeder system for the Greenstone Flow. The large areal ex-  
 28 tent and estimated volume of the intrusives and volcanics suggest that they represent  
 29 a rapid and voluminous *ca.* 1092 Ma magmatic pulse near the end of the main stage of  
 30 Midcontinent Rift magmatism.  
 31

32 **1 Introduction**

33 The North American Midcontinent Rift is a *ca.* 1.1 Ga large igneous province for  
 34 which there is excellent exposure of both the intrusive and extrusive components in the  
 35 Lake Superior region (Fig. 1). An exceptional feature of the Midcontinent Rift is the oc-  
 36 currence of large anorthosite xenoliths (whose diameter can exceed 100 meters) within  
 37 a diabase sill and dike network known as the Beaver River diabase that outcrops in north-  
 38 eastern Minnesota, USA as part of the Beaver Bay Complex (Fig. 1). Despite these anorthosite  
 39 xenoliths having long been recognized and mapped, the origin of these nearly pure pl-  
 40 gioclase cumulates has been debated in the literature (Lawson, 1893; Grout, 1939; Mor-  
 41 rison et al., 1983; Miller & Chandler, 1997). Lacking the roadcut exposures that now make  
 42 the xenolithic relationship clear and observing the large blocks exposed along the Lake  
 43 Superior shoreline and at Carlton Peak, Lawson (1893) did not recognize the xenolithic  
 44 nature of the anorthosites. Rather, he argued that the anorthosite is Archean in age and  
 45 that the Keweenawan (i.e. Midcontinent Rift related) magma was emplaced atop an anorthosite  
 46 erosional unconformity surface. Later work established the anorthosite blocks as xeno-

47 liths, which is now very well-documented through geologic mapping of the region (Fig.  
48 1; Miller et al. (2001); Miller (1988); Miller and Boerboom (1989); Boerboom (2004); Boer-  
49 boom and Green (2006); Boerboom et al. (2006, 2007)) and outcrop-scale exposures (Fig.  
50 2).

51 The anorthosite xenoliths range in size from centimeter-scale megacrysts to meter-  
52 scale, decimeter-scale and even >100 meter-scale blocks (Fig. 2). There have been di-  
53 vergent interpretations regarding the age and magma source of these anorthosite xeno-  
54 liths (Fig. 1). Grout (1939) recognized the xenolithic nature of the anorthosites and sug-  
55 gested that the massive intrusion of the older anorthositic gabbro within the Duluth Com-  
56 plex may have supplied anorthosite fragments that were later entrained by the Beaver  
57 River diabase emplacement. However, there are grain size and textural differences be-  
58 tween the anorthosite xenoliths and the anorthositic series of the Duluth Complex that  
59 challenge this interpretation. Morrison et al. (1983), on the other hand, argued that the  
60 xenoliths were sourced from Paleoproterozoic or Archean lower crust that was liberated  
61 by Midcontinent Rift magma based on Sr and Nd isotopic data from the anorthosites.  
62 That study argued that similarities in isotopic data between the anorthosites and other  
63 Midcontinent Rift lithologies resulted from contamination by Keweenawan magmas. They  
64 interpret a Sm/Nd model age of 1.9 Ga from one of the xenoliths as providing a min-  
65 imum crystallization age for the anorthosites. In contrast to this Archean to Paleopro-  
66 terozoic model, Miller and Chandler (1997) favored a scenario where the anorthosite crys-  
67 tallized as part of Midcontinent Rift magmatism. They envision that the anorthosite xeno-  
68 liths represent crystal mushes that were generated in lower crustal magma chambers dur-  
69 ing Midcontinent Rift development. The density contrast between plagioclase and tholei-  
70 itic magma under high temperature and high pressure conditions of the lower crust pro-  
71 motes the precipitation and segregation of plagioclase from the parent magma, leading  
72 to the flotation of anorthosite (Kushiro, 1980). This mechanism can concentrate plago-  
73 clase into anorthosite cumulates in the roof zone of lower crustal magma chambers. Miller  
74 and Chandler (1997) also argue that the isotopic data of Morrison et al. (1983) is am-  
75 biguous and can be explained by anorthosite-forming Midcontinent Rift magmas hav-  
76 ing been contaminated by older crust rather than the anorthosites being older crust that  
77 was contaminated by Midcontinent Rift magmas.

78 Regardless of their origin, the exceptional sizes of some of the anorthosite xeno-  
79 liths reveal the gigantic sizes of the Beaver River diabase conduits. A particularly large

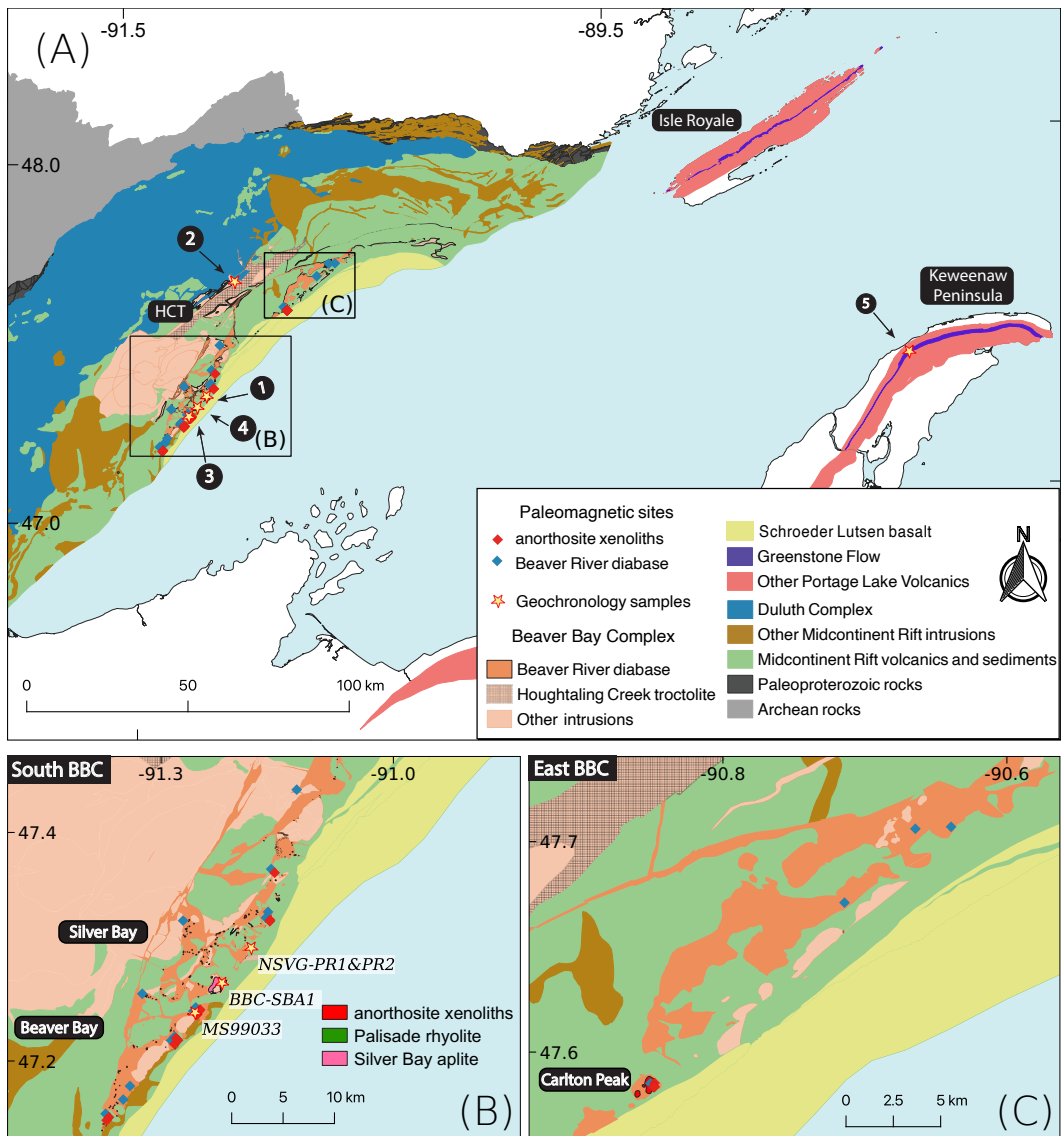


**Figure 1.** (A) Geologic map of exposures of Midcontinent Rift volcanics and intrusives in the western Lake Superior region. The Greenstone Flow of the Portage Lake Volcanics that outcrops throughout the Keweenaw Peninsula and Isle Royale is highlighted in purple. (B) Regional map of paleomagnetic and geochronologic sites in the southern Beaver Bay Complex (south BBC). Note that paleomagnetic site AX16 and geochronologic sample MS99033 are from the same anorthosite xenolith. The geochronology sample numbers in (A) and (B) correspond to those in Figure 6. (C) Regional map of paleomagnetic sites in the eastern Beaver Bay Complex (east BBC). The xenolith at Carlton Peak is >100 meters in diameter. The younger Schroeder-Lutsen basalt of the North Shore Volcanic Group (NSVG) is lying unconformably atop the Beaver River diabase and other NSVG units. The nomenclature of the “southern” and “eastern” Beaver Bay Complex follows Miller and Chandler (1997). Bedrock geology is from Miller et al. (2001) and Jirsa et al. (2011).

80 anorthosite xenolith is exposed at Carlton Peak in the eastern Beaver Bay Complex with  
81 minimum dimensions of  $180 \times 240$  meters (Boerboom et al. (2006); Fig. 1, 2). In the  
82 southern Beaver Bay Complex, a large anorthosite xenolith near Corundum Point has  
83 dimensions of  $180 \times 230$  meters while the one exposed at Split Rock Point has dimen-  
84 sions of  $180 \times 260$  meters (Boerboom, 2004). To be able to accommodate such large xeno-  
85 liths during magma ascent, the Beaver River diabase conduits must have been of at least  
86 the width of the anorthosite short axis diameters. Such wide conduits in these near-surface  
87 intrusions suggest high magma flux rates and make it likely that the magma extruded  
88 to the surface — feeding voluminous lava flows.

89 One such intrusive-extrusive correlation could have existed between the Beaver River  
90 diabase and the Greenstone Flow which is the largest single lava flow in the Portage Lake  
91 Volcanic group (Fig. 1) and one of the largest lava flows on Earth (Fig. 3). The Green-  
92 stone Flow is a massive basalt flow that extends laterally for  $\sim 90$  kilometers on the Ke-  
93 weenaw Peninsula with a maximum thickness of  $\sim 450$  meters (Fig. 1, White (1960)).  
94 The same flow is found  $\sim 80$  km to the northwest on Isle Royale where it extends along  
95 the entirety of the island for  $\sim 80$  kilometers and has a maximum thickness of  $\sim 250$  me-  
96 ters (Fig. 1; Huber (1973)). Longo (1984) calculated a minimum estimate of  $\sim 1650$  km<sup>3</sup>  
97 for the volume of the Greenstone Flow — a minimum as the flow could extend laterally  
98 well beyond the Keweenaw Peninsula and Isle Royale. This volume makes it one of the  
99 largest documented mafic lava flows on Earth (Fig. 3). The Beaver River diabase with  
100 its wide conduits could have been the feeder system to this lava flow which is consistent  
101 with their similar lithologies. Miller and Chandler (1997) and Doyle (2016) proposed that  
102 the Beaver River diabase and the Greenstone Flow were comagmatic based on their sim-  
103 ilar petrographic characteristics and geochemical compositions of the plagioclase megacrysts  
104 and the fresh pyroxene and olivine crystals. Such a comagmatic relationship is consis-  
105 tent with the similar  $^{207}\text{Pb}/^{206}\text{Pb}$  dates developed from a granophyric ferrogabbro within  
106 the Beaver Bay Complex ( $1095.8 \pm 1.2$  Ma, Paces and Miller (1993)) and the Greenstone  
107 Flow ( $1094.0 \pm 1.5$  Ma, Davis and Paces (1990)). However, these dates have relatively  
108 large uncertainties such that the temporal relationship between the units is more roughly  
109 constrained than is possible with modern methods.

110 Modern-day U-Pb geochronology techniques for isotope dilution-thermal ioniza-  
111 tion mass spectrometry (ID-TIMS) allow high precision  $^{206}\text{Pb}/^{238}\text{U}$  dates to be devel-  
112 oped from chemically-abraded zircon crystals (Mattinson, 2005). Studies utilizing these

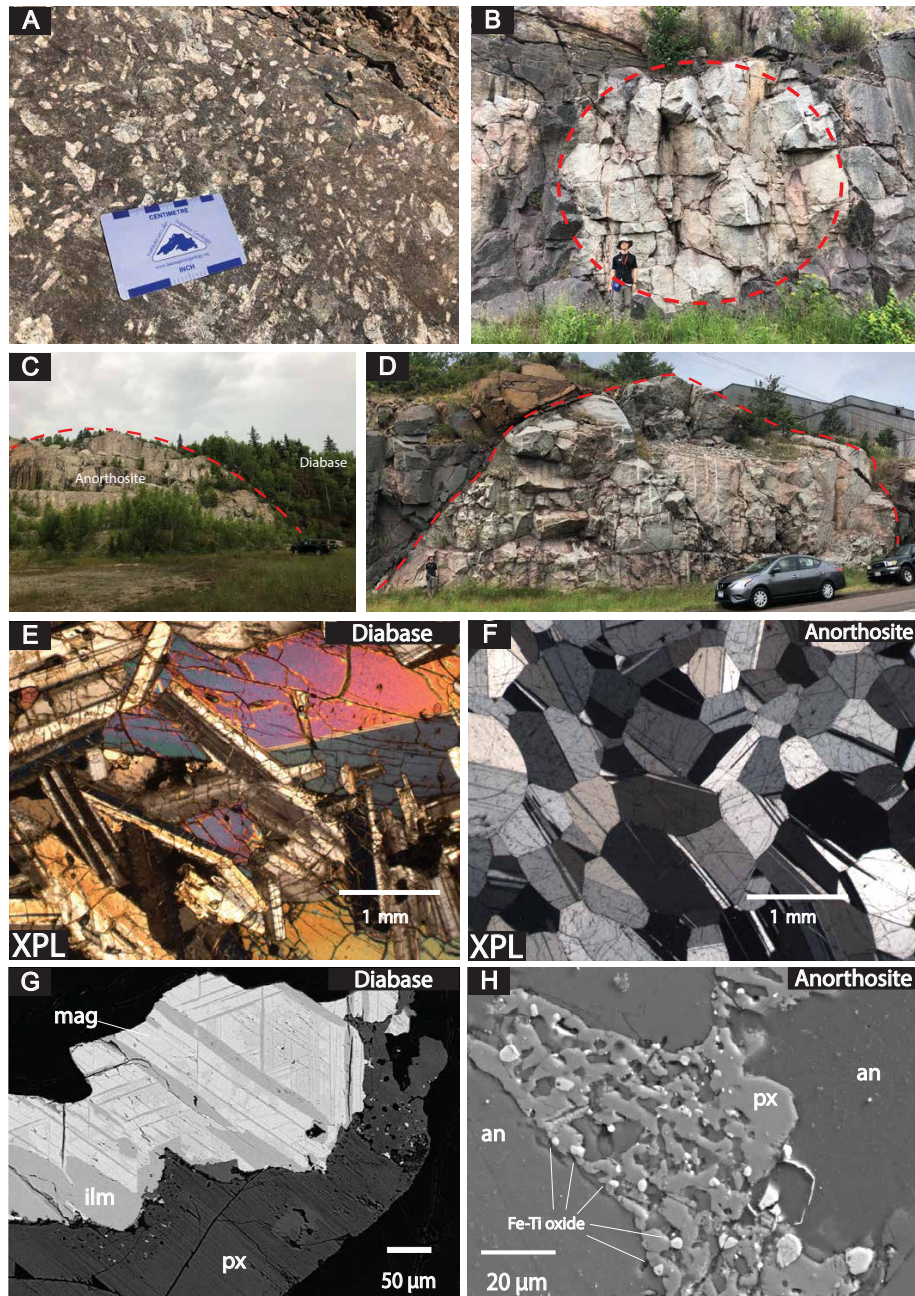


**Figure 2.** Field photographs and petrographic images of the Beaver River diabase and the anorthosite xenoliths within it. (A) Centimeter-sized plagioclase megacrysts in the diabase. (B) Rounded anorthosite xenolith with a diameter of 7 meters fully entombed within the diabase. (C) Exposure of a giant Carlton Peak anorthosite with a diameter  $>100$  m. (D) 27.5 m diameter anorthosite xenolith sampled as paleomagnetic site AX16 and geochronology sample MS99033. (E) Cross polarized (XPL) image of the subophitic texture of the diabase (pyroxene partially enclosing plagioclase). (F) XPL image of an anorthosite dominated by subequant plagioclase crystals. (G) Back scattered electron (BSE) image of a large Fe-Ti oxide with titanomagnetite-ilmenite lamellae in the diabase. (H) BSE image of micron-sized Fe-Ti oxides exsolved from pyroxene between plagioclase crystals in an anorthosite sample.

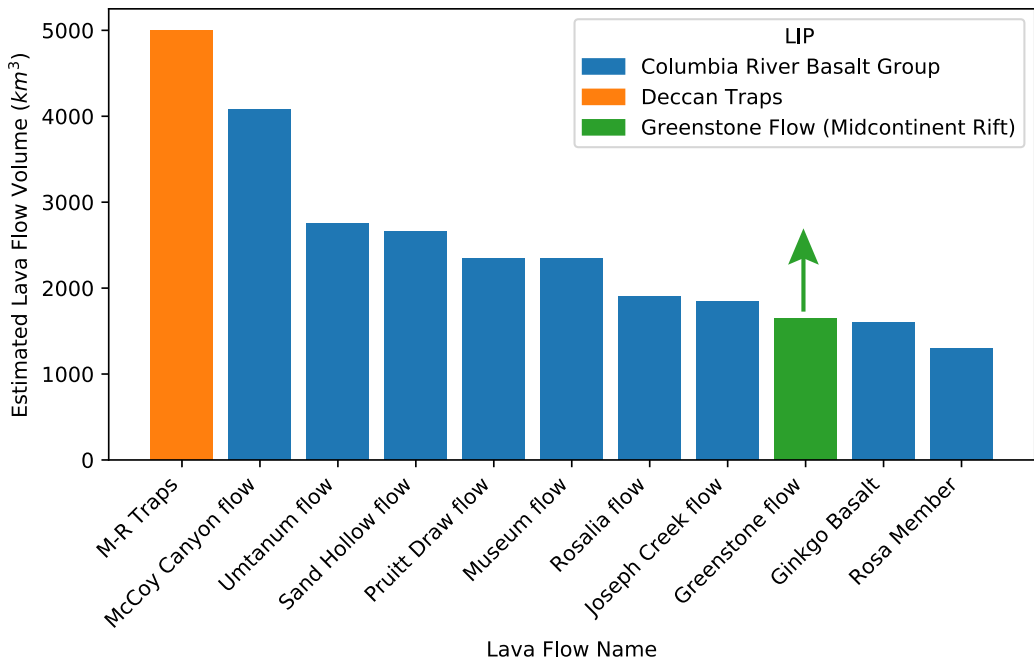


**Figure 3.** Bar plot of ten of the world's most voluminous known single mafic lava flows. With an estimated minimum volume of  $\sim 1650 \text{ km}^3$ , the Greenstone Flow from the 1.1 Ga Midcontinent Rift stands amongst the giant lava flows from the Deccan Traps and Columbia River basalts. M-R Traps-Mahabaleshwar–Rajahmundry lava flow in the Deccan Traps. Data from Self et al. (2008), Bryan et al. (2010) and Longo (1984).

113 methods on Midcontinent Rift volcanics and intrusions have shown that the analytical  
114 uncertainties on weighted mean  $^{206}\text{Pb}/^{238}\text{U}$  dates of chemically-abraded single zircons  
115 can have sub-million year uncertainty, an order of magnitude smaller than previous dates  
116 (Fairchild et al., 2017; Swanson-Hysell et al., 2019, 2020). Such precision can give bet-  
117 ter insights into rates of magmatic activity and the feasibility of proposed relationships  
118 between intrusive and extrusive units. In this work, we develop a  $^{206}\text{Pb}/^{238}\text{U}$  zircon date  
119 for an anorthosite xenolith to evaluate models of the origin of the xenoliths and the re-  
120 lationship between the Beaver River diabase and the Greenstone Flow.

121 Paleomagnetic data can also provide chronological constraints on rock units. Lau-  
122 rentia experienced a period of rapid latitudinal plate motion during rift development (Swanson-  
123 Hysell et al., 2009). A synthesized apparent polar wander path (APWP) based on the  
124 Midcontinent Rift volcanic rocks indicates that motion exceeded 20 cm/yr (Swanson-  
125 Hysell et al., 2019), faster than the maximum speed of India of  $\sim$ 17 cm/yr during the  
126 Cenozoic (van Hinsbergen et al., 2011). This motion resulted in significant differences  
127 in pole positions recorded by Midcontinent Rift rocks that were emplaced a few million  
128 years apart (Swanson-Hysell et al., 2019). In this study, we present paleomagnetic data  
129 from the anorthosite xenoliths and the host Beaver River diabase. Data from the xeno-  
130 liths give equivalent directions to the host diabase (Figs. 4 and 5), indicating that they  
131 were heated above the Curie temperature of magnetite and acquired a thermal rema-  
132 nent magnetization when they cooled with the diabase. This thermal history is consis-  
133 tent with thermal diffusion modeling of the xenoliths. The paleomagnetic data can be  
134 compared to data from the Greenstone Flow to further test the hypothesis that they are  
135 synchronous. The resulting paleomagnetic pole positions can also be compared to the  
136 synthesized Laurentia APWP to obtain chronological constraints (Fig. 5).

137 Here, by integrating the geochronologic and paleomagnetic perspectives with pre-  
138 vious geochemical analyses (Miller & Chandler, 1997; Doyle, 2016), we establish the Beaver  
139 River diabase network as the feeder system for the Greenstone Flow. Their shared geo-  
140 chemical signatures, composite nature of emplacement, and giant magma conduits to-  
141 gether characterize a period of *ca.* 1092 Ma voluminous magmatic activity after the *ca.*  
142 1096 Ma formation of the Duluth Complex (Fig. 1).

143 **2 Geologic Setting**144 **2.1 The Beaver Bay Complex**

145 The North American Midcontinent Rift System is a failed intracontinental rift where  
 146 protracted magmatic activity lasted for more than 20 million years from before *ca.* 1105  
 147 Ma to after *ca.* 1085 Ma (Swanson-Hysell et al., 2019). Midcontinent Rift rocks exten-  
 148 sively outcrop in today's Lake Superior region, with the total extent traceable by arcu-  
 149 ate magnetic and gravity anomalies that extend to the southwest to Kansas to the south-  
 150 east to southern Michigan (Hinze & Chandler, 2020). Previous studies have divided mag-  
 151 matic activity in the rift into four stages based on changes in relative volcanic volume  
 152 and the nature of magmatism: early ( $\sim$ 1109–1104 Ma), latent ( $\sim$ 1104–1098 Ma), main  
 153 ( $\sim$ 1098–1090 Ma) and late ( $\sim$ 1090–1083 Ma) (Vervoort et al., 2007; Miller & Ripley, 1996;  
 154 Davis & Green, 1997).

155 The Beaver Bay Complex is one of the intrusive complexes that resulted from main  
 156 stage magmatism. The exposed area of the Beaver Bay Complex is  $\sim$ 1,000 km<sup>2</sup> where  
 157 it has been mapped along the northwestern shore of Lake Superior in northeastern Min-  
 158 nesota (Fig. 1, Supporting Information). The Beaver Bay Complex is a hypabyssal, multi-  
 159 phase, composite intrusive complex that intrudes the North Shore Volcanic Group and  
 160 is higher in the stratigraphy than the older *ca.* 1096 Ma Duluth Complex (Fig. 1, Miller  
 161 and Chandler (1997); Swanson-Hysell et al. (2020)). Detailed mapping and petrologi-  
 162 cal analyses of the Beaver Bay Complex has led to the identification of thirteen intru-  
 163 sive units and at least six major intrusive events (Miller & Chandler, 1997). The com-  
 164 plex has a shallow southerly dip toward the lake basin, similar to that of the North Shore  
 165 Volcanic Group (Miller et al., 2001). An augite troctolite near Houghtaling Creek (HCT)  
 166 in the northwest boundary is interpreted to be the oldest unit of the Beaver Bay Com-  
 167 plex (Fig. 1). However, a  $^{206}\text{Pb}/^{238}\text{U}$  date of  $1095.44 \pm 0.26$  Ma from Swanson-Hysell  
 168 et al. (2020) indicates that the age of this unit is closer to the layered series of the Du-  
 169 luth Complex rather than the other units in the Beaver Bay Complex. This date is con-  
 170 sistent with the interpretation of Miller and Chandler (1997) that the Houghtaling Creek  
 171 troctolite is cogenetic with the Duluth Complex layered series based on the troctolite's  
 172 close proximity to the roof zone rocks of the Duluth Complex, and the merging pattern  
 173 on the aeromagnetic anomaly data between the Duluth layered series and the troctolite  
 174 unit. Miller and Chandler (1997) also interpreted that the Wilson Lake ferrodiorite of

the Beaver Bay Complex to the north of Houghtaling Creek troctolite to be of an older age. However, a  $^{206}\text{Pb}/^{238}\text{U}$  date of  $1091.63 \pm 0.35$  Ma reveals that it is younger and is similar in age to other Beaver Bay Complex intrusions (Swanson-Hysell et al., 2020). Elsewhere in the Beaver Bay Complex, dikes and sills of the non-cumulate ophitic to sub-ophitic Beaver River diabase is the most areally extensive unit, which has the unique feature of bearing anorthosite xenoliths (Fig. 1, 2). In the southern part of the Beaver Bay Complex, the diabase occurs as dikes and sills, typically including anorthosites with various sizes ranging from centimeters to over one hundred meters (Figs. 1, 2). The diabase in this region intrudes the Palisade rhyolite of the North Shore Volcanic Group (Fig. 1), which has a  $^{206}\text{Pb}/^{238}\text{U}$  date of  $1093.94 \pm 0.28$  Ma (Swanson-Hysell et al., 2019). The Beaver River diabase is intruded by the Silver Bay intrusions (Fig. 1), which are the youngest intrusive bodies of the southern Beaver Bay Complex (Miller & Chandler, 1997). An aplite unit within the granophyre zone of one of these Silver Bay intrusions has a  $^{206}\text{Pb}/^{238}\text{U}$  date of  $1091.61 \pm 0.14$  Ma (Swanson-Hysell et al., 2019). Another arcuate, sill-like diabase body mapped as the Beaver River diabase outcrops along the eastern part of the complex (Fig. 1). The diabase composition there is similar to that in southern exposures and it also contains large anorthosite xenoliths that exceed 100 meters at Carlton Peak. The Beaver River diabase in the northern part of the Beaver Bay Complex near the Houghtaling Creek area occurs as steeply-walled dikes instead of sheets in the southern and eastern regions, and rarely contains large anorthosite xenoliths (Fig. 1, Miller and Chandler (1997)).

Hundreds of anorthosite xenoliths has been recognized and mapped within the Beaver River diabase (Fig. 1). Many hill tops in the Beaver Bay Complex, such as the Carlton Peak and Britton Peak, are large anorthosite blocks (which lead Lawson (1893) to erroneously conclude that they were relict Archean topography). In the field, the anorthosites typically appear as subrounded to rounded, light-colored, translucent blocks that are in sharp contact with the hosting diabase (Fig. 2). They also occur as exposures whose contact with the diabase is covered (Fig. 2). Grout (1939) suggested that the rounded anorthosites are the result of friction during transportation as they were liberated by the diabase (i.e. physical weathering within a magmatic system). While the Beaver River diabase is chilled against the North Shore Volcanic Group lithologies that it intrudes, the diabase is not chilled against the margin of the anorthosite xenoliths (Morrison et al., 1983; Miller & Chandler, 1997). The lack of chilled contacts is consistent with the anorthosite having

reached elevated temperatures within the diabase magma during emplacement. Based on unpublished X-ray diffraction data, Miller and Chandler (1997) interpreted that the anorthosites have a high state of structural disorder, which supports the interpretation of a deep crustal source where pressure is high and plagioclase was buoyant in magma due to relatively low density. This interpretation is inspired by experimental data from Kushiro (1980) which found that because of the greater compressibility of liquids over solids, the density of solid plagioclase will be less than that of basaltic magma at pressures of the lower crust. These properties can result in the flotation of plagioclase and the creation of anorthositic cumulates in the cupolas of lower crustal magma chambers.

The anorthosite xenoliths are dominantly monomineralic plagioclase that has an anorthite content of ~70% (Morrison et al., 1983; Doyle, 2016). Augite and olivine are present in minor concentrations in the xenoliths. Within the Carlton Peak anorthosite xenolith, up to 10 cm pockets of dotted and altered mafic minerals such as olivine can occur. Nevertheless, the overall olivine content in the anorthosites is small. Interstitial titanomagnetite-ilmenite intergrowths that exceed 100 microns can be found through microscopy and less than twenty-micron-sized Ti-Fe oxide grains can be detected with scanning electron microscopy (Fig. 2). Some of the anorthosites have an equigranular texture with hexagonal-shaped crystals (Fig. 2). This texture suggests that the plagioclase underwent recrystallization at elevated temperatures, consistent with the interpretation that they were liberated and heated by the emplacement of the Beaver River diabase. In addition, microscopic deformation textures, such as undulose extinctions and deformation twins that developed within plagioclase crystals in some of the xenoliths suggest that the anorthosites were heated and deformed at high temperatures. Anorthosites with higher degrees of recrystallization contain fewer Fe-Ti oxides than those with lower degrees. The correlation between the recrystallization textures and the interstitial melt content fits the scenario where the mafic interstitial material in the plagioclase cumulate was partially removed as the anorthosite xenoliths were heated.

## 2.2 The Greenstone Flow

The Greenstone Flow of the Portage Lake Volcanic Group has been recognized as one of the largest lava flows on earth, with an estimated volume likely exceeding 1650 km<sup>3</sup> (Fig. 1, Longo (1984)). It outcrops along the Keweenaw Peninsula and Isle Royale. The flow can be correlated between the two outcrop regions on the basis of geochemi-

240 cal, petrographic and paleomagnetic similarity of the flow itself and the flows above and  
 241 below (Longo, 1984). In both outcrop regions, the Greenstone Flow is underlain by con-  
 242 glomerate and overlain by pyroclastic breccia (Lane, 1911; Huber, 1973). On the Keweenaw  
 243 Peninsula, the Greenstone Flow is exposed over 90 km and reaches a maximum thick-  
 244 ness of over 450 meters, dipping to the northwest (Fig. 1, White (1960)). On Isle Royale,  
 245 the Greenstone Flow has a maximum thickness of about 250 meters with a shallower dip  
 246 toward the southeast (Fig. 1, Huber (1973)).

247 According to the mineralogical and textural attributes, Doyle (2016) divided the  
 248 Greenstone Flow into four zones from bottom to top — lower ophitic zone, heterolithic  
 249 zone, upper ophitic zone, and an amygdaloidal zone. Field observations, geochemical anal-  
 250 yses and parent magma calculations conducted by Doyle (2016) suggest that the zoned  
 251 Greenstone Flow formed through an open-system differentiation of a composite parent  
 252 magma which is more evolved than the primitive olivine tholeiites generated by the Mid-  
 253 continent Rift plume. That study proposed that the emplacement of the Greenstone Flow  
 254 started with a voluminous eruption of olivine tholeiitic magma, forming the ophitic zones  
 255 which subsequently inflated due to the intrusions of more evolved basaltic magma which  
 256 composes the heterolithic zone. A final stage of localized melt migration and differen-  
 257 tiation resulted in the heterogeneous composition of the heterolithic zone. A  $^{206}\text{Pb}/^{238}\text{U}$   
 258 zircon date of  $1091.59 \pm 0.27$  Ma for the Greenstone Flow was developed from a peg-  
 259 matoid sample from the heterolithic zone (Swanson-Hysell et al., 2019).

### 260 3 Methods and Results

#### 261 3.1 Paleomagnetism

262 We sampled standard paleomagnetic cores along the southern and eastern Beaver  
 263 Bay Complex with a particular focus on acquiring paired sites of anorthosite xenoliths  
 264 and their local diabase hosts. Sample cores were collected using a hand-held gasoline-  
 265 powered drill and were oriented using a magnetic compass as well as a sun compass when  
 266 possible. Sun compass orientations were preferentially used for determining the sample  
 267 azimuth. Typically, 7-10 cores were drilled for each anorthosite xenolith and their dia-  
 268 base hosts. A total of 17 diabase sites and 22 anorthosite sites were collected (Table 1).  
 269 A table that summarizes the known dimensions of each anorthosite xenolith sampled and

270 the distance between each anorthosite paleomagnetic site and closest diabase host site  
 271 is provided in the Supporting Information.

272 Samples underwent step-wise demagnetization and analyses in the magnetically shielded  
 273 room in the UC Berkeley Paleomagnetism Lab. 7 sites from the Beaver River diabase  
 274 underwent alternating field (AF) demagnetization with peak fields from 1 mT to 130 mT.  
 275 An ASC TD-48SC thermal demagnetizer was used to demagnetize 10 diabase sites and  
 276 all 22 anorthositic sites in a step-wise manner, with reduced step increments between 540  
 277 °C and 585 °C. The typical magnetic field inside the shielded room is <500 nT and the  
 278 field inside the thermal demagnetizer chamber is <10 nT. The quartz glass sample rod  
 279 of the UC Berkeley system is typically measured at  $5 \times 10^{-12}$  Am<sup>2</sup>. All remanence mea-  
 280 surements were made on a 2G Enterprises DC-SQUID superconducting rock magnetome-  
 281 ter equipped with inline AF coils and an automated sample changer system. The PmagPy  
 282 software package was used implement the least-square fits for specimen demagnetization  
 283 data (Tauxe et al., 2016). Measurement level data are available within the MagIC database  
 284 *for the purposes of review, these data are available in a pre-publication contribution within*  
*285 the MagIC database that can be accessed here: <https://earthref.org/MagIC/17102/400e0fb3-a79b-42bd-aeab-9005d2e3b438>*  
 286

287 For both the diabase and anorthositic, vector component analyses of their demag-  
 288 netization data show that an origin trending characteristic remanent magnetization (ChRM)  
 289 can be isolated after the removal of a minimal secondary component during the first few  
 290 low coercivity (< 10 mT) or low temperature (<200 °C) demagnetization steps (Fig. 4).  
 291 The ChRMs typically unblock through thermal demagnetization steps from ~500 °C to  
 292 ~580 °C, consistent with them being held by titanomagnetite. We interpret this com-  
 293 ponent as a primary remanent magnetization acquired during the emplacement and cool-  
 294 ing of the Beaver River diabase.

295 The site mean paleomagnetic directions are shown in Table 1. We present both AF  
 296 and thermal demagnetization results for the Beaver River diabase as both methods are  
 297 effective in removing the secondary components and isolating the coherent and univec-  
 298 toral ChRM. Based on specimen and site level demagnetization behavior and the prox-  
 299 imity between paired paleomagnetic sites of the anorthositic xenoliths and the diabase,  
 300 we grouped the anorthositic xenoliths and their diabase hosts into individual cooling units

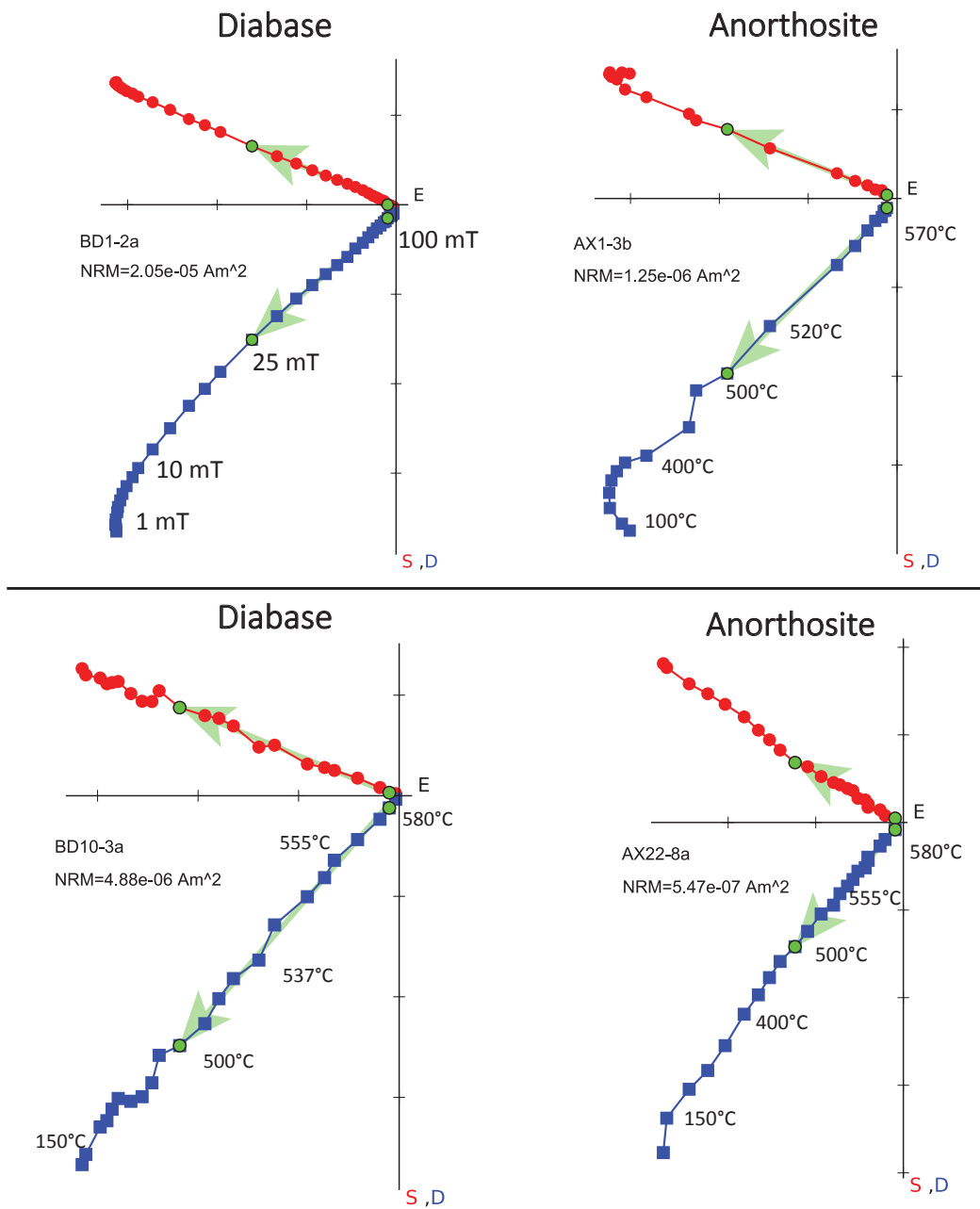


**Figure 4.** Example orthogonal vector demagnetization diagrams for diabase and anorthosite specimens. Anorthosite site AX1 is from a xenolith within the diabase sampled as BD1. Similarly, AX22 is from a xenolith with the BD10 diabase. Both AF and thermal demagnetization show dominantly univectoral decay of characteristic remanent magnetizations (ChRM) toward the origin after removal of minimal secondary components. The example specimen results show very similar ChRM directions between the paired diabase and anorthosite xenoliths sites.

301 and calculated a paleomagnetic pole position as the mean of the cooling unit virtual ge-  
 302 omagnetic poles (Supporting Information).

303 Tilt-correcting the paleomagnetic directions to paleohorizontal is necessary for de-  
 304 veloping accurate paleomagnetic poles from the diabase and the anorthosite xenoliths  
 305 to be compared to the Keweenawan apparent polar wander path (Fig. 5, Swanson-Hysell  
 306 et al. (2019)). For intrusive igneous rocks, this can be difficult due to the intrinsic lack  
 307 of paleohorizontal reference. Many paleomagnetic studies of Midcontinent Rift intrusive  
 308 rocks in the Lake Superior region did not apply tilt corrections to their data (e.g., Beck  
 309 & Lindsley, 1969; Beck, 1970; Books et al., 1966). However, we can determine the struc-  
 310 tural orientation of the Beaver River diabase using the abundant igneous fabric ori-  
 311 entations measured on the diabase as well as bedding orientations measured from its ad-  
 312 jacent volcanic units (Boerboom, 2004; Boerboom & Green, 2006; Boerboom et al., 2006,  
 313 2007; Miller et al., 2001). We compile the igneous layering measurements from the Beaver  
 314 River diabase and the volcanic bedding orientations from the Schroeder-Lutsen basalt  
 315 which is overlying the Beaver Bay Complex. The mean tilt orientations of both units are  
 316 similar (diabase dip trend/dip: 128.5/10.2; basalt dip trend/dip: 142.2/13.6). We com-  
 317 bine the structural measurements from the Beaver River diabase and the Schroeder-Lutsen  
 318 basalt and derived two sets of tilt corrections for the paleomagnetic directions of the di-  
 319 abase and anorthosite (dip trend/dip in the southern Beaver Bay complex: 128.7/12.9;  
 320 in the eastern Beaver Bay Complex: 145.6/13.1, Supporting Information). The advan-  
 321 tage of using the structural orientations from the Schroeder-Lutsen basalt is that the ar-  
 322 cuate shape of the Beaver River diabase intrusions is nicely captured by the variation  
 323 of basalt dip directions while the dip angles of the basalt and diabase are very similar(Fig.  
 324 1).

325 The tilt-corrected ChRMs in both lithologies are northwest and down, yielding good  
 326 specimen-level and site-level consistency (Fig. 4, 5). Close directional similarities between  
 327 each anorthosite xenolith and their host diabase are supported by 9 out of a total of 17  
 328 diabase-anorthosite paleomagnetic site pairs passing a common mean test (McFadden  
 329 & McElhinny, 1990). The overall mean directions between the two lithologies are indis-  
 330 tinguishable as they also pass a common mean test (Figure 5, McFadden and McElhinny  
 331 (1990)). For the anorthosite sites that do not pass a common mean test with their di-  
 332 abase hosts, they nevertheless have coherent specimen-level directions that are close to  
 333 their host diabase directions (Fig. 5). We also plot the tilt-corrected mean pole of sites

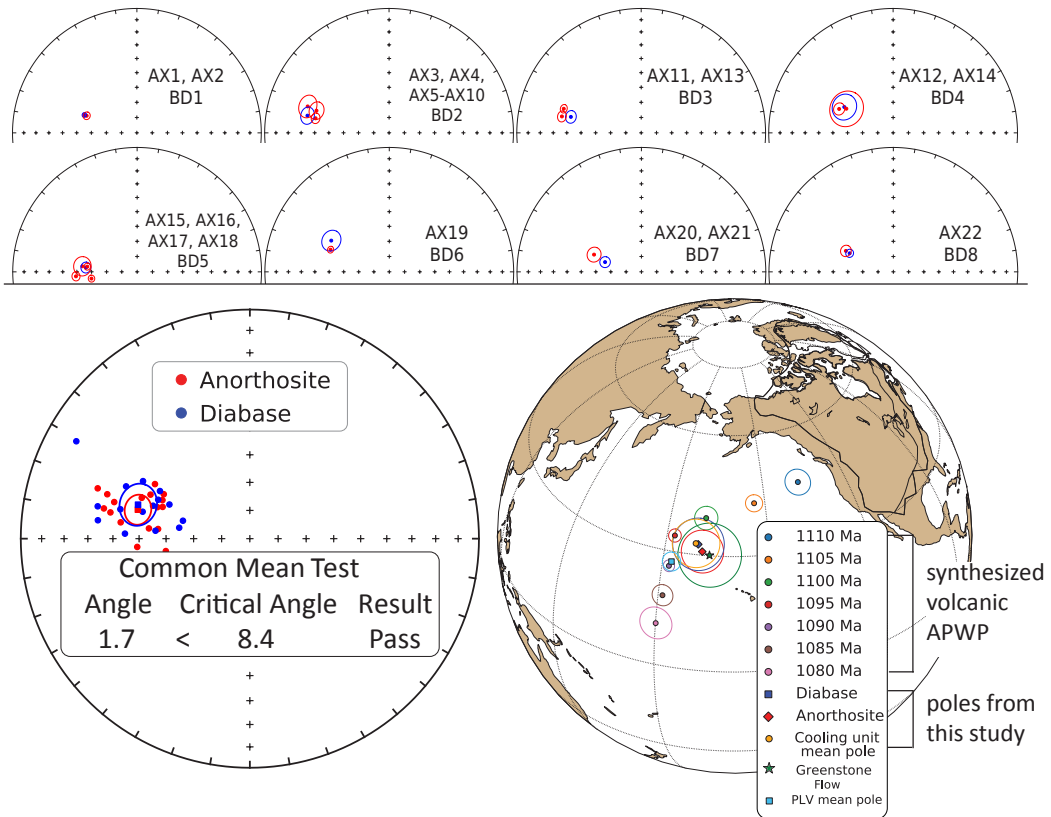


**Figure 5.** Top: Equal area plots of paleomagnetic directions from the anorthosite xenoliths and their local diabase hosts. Bottom: Site mean paleomagnetic directions from the Beaver River diabase and anorthosite xenoliths are plotted on equal area plots. The anorthosite and diabase sites share a common mean as summarized by the results of the McFadden and McElhinny (1990) common mean test. Mean paleomagnetic pole positions of all diabase sites, all anorthosite sites, as well as a grand mean pole developed by grouping the anorthosite and diabase sites into individual cooling units are plotted against the synthesized Laurentia APWP based on poles from Midcontinent Rift volcanics and sedimentary rocks (Swanson-Hysell et al., 2019). The combined paleomagnetic poles from the diabase and anorthosite is indistinguishable with the Greenstone Flow pole developed by Foucher (2018). However, the mean paleomagnetic pole of the Portage Lake Volcanics (PLV mean pole) is close to but distinct from them. All directions shown are tilt corrected.

334 from both lithologies (diabase: 32.5°N, 189.5°E, N = 15, A95 = 6.3, k = 37.4; anorthosite:  
 335 30.9°N, 190.8°E, N = 17, A95: 5.2, k = 48.5) in context of a previously synthesized ap-  
 336 parent polar wander path (APWP) from the volcanics of the Midcontinent Rift (Swanson-  
 337 Hysell et al., 2019) and show the poles lie near the expected 1090 Ma and 1095 Ma pole  
 338 positions (Fig. 5). The mean pole position of the interpreted cooling units (32.7°N, 188.8°E,  
 339 N = 15, A95 = 5.9, k = 41) lies close to the mean pole position derived from the *ca.* 1092  
 340 Ma Portage Lake Volcanics (Fig. 5), consistent with the coeval magmatic activity be-  
 341 tween the Beaver River diabase and the Portage Lake Volcanics. This cooling unit mean  
 342 pole is recommended to be used to as a pole for the Beaver River diabase in future Lau-  
 343 rentia Midcontinent Rift APWP compilations.

### 344 3.2 Geochronology

345 A sample of an anorthosite xenolith within the Beaver River diabase was collected  
 346 for U-Pb geochronology along Hwy 61 across from the Silver Bay taconite plant (MS99033;  
 347 91.26358°W 47.28888°N; Figure 1). This sample comes from the same xenolith sampled  
 348 for paleomagnetic study as site AX16 which has an exposed diameter of 27.5 meters (Fig-  
 349 ure 2). Zircons were separated from a kilogram of the anorthosite using common min-  
 350 eral separation methods (Supporting Information). The separated zircons were subhe-  
 351 dral to anhedral crystals (z1-z4) and platy fragments (z5-z8). The subhedral to anhedral  
 352 crystals are consistent with intercumulus crystallization within an adcumulate with platy  
 353 fragments also being a common zircon morphology within the Duluth Complex anorthositic  
 354 series (e.g. samples AS-1 and FC-1 of Paces and Miller (1993)). Eight chemically-abraded  
 355 zircons were analyzed by isotope dilution-thermal ionization mass spectrometry (ID-TIMS)  
 356 in the Boise State Isotope Geology Laboratory using EARTHTIME tracer solutions (Condon  
 357 et al., 2015). Both zircon morphologies yield indistinguishable dates. Using six of these  
 358 single grain dates (and excluding two due to interpreted Pb-loss) results in a weighted  
 359 mean  $^{206}\text{Pb}/^{238}\text{U}$  date of  $1091.83 \pm 0.21/0.37/1.15$  Ma (analytical/ analytical+tracer/  
 360 analytical+tracer+decay uncertainty; Figure 6).

361 This date provides a tight constraint on the age of the Beaver River diabase. Pre-  
 362 viously, the maximum age constraint for the Beaver River diabase came from the rela-  
 363 tionship that it cross-cuts the Palisade rhyolite of the North Shore Volcanic Group which  
 364 has a  $^{206}\text{Pb}/^{238}\text{U}$  date of  $1093.94 \pm 0.28$  Ma (Swanson-Hysell et al., 2019). With this  
 365 new date, we know the crystallization age of the diabase to have been near-synchronous

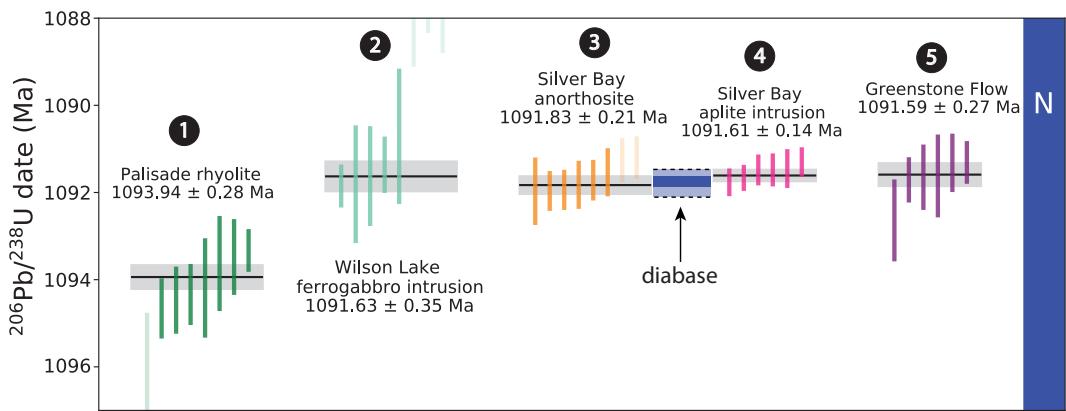


**Figure 6.** New  $^{206}\text{Pb}/^{238}\text{U}$  zircon date of the anorthositic xenolith (orange) plotted in context of previously published ages from the North Shore Volcanic Group (NSVG) and other Beaver Bay Complex intrusions. The high-resolution geochronology data are consistent with field observations that the Beaver River diabase crosscuts the Palisade rhyolite and is cut by the Silver Bay intrusions. The dates for the Greenstone Flow of the Portage Lake Volcanics, the Beaver River diabase, the Wilson Lake ferrogabbro, and a Silver Bay intrusion aplite are indistinguishable. Each vertical bar corresponds to one  $^{206}\text{Pb}/^{238}\text{U}$  date from a single zircon crystal. The translucent bars represent zircons with interpreted Pb loss and are therefore not included in the mean age calculations. Horizontal lines and gray boxes represent weighted mean dates and their uncertainty.

366 or younger with the date of the anorthositic xenolith ( $1091.83 \pm 0.21$  Ma). The Silver  
 367 Bay intrusions, from which an aplite has a  $^{206}\text{Pb}/^{238}\text{U}$  date of  $1091.61 \pm 0.14$  Ma, (Fairchild  
 368 et al., 2017), cross-cut the Beaver River diabase. These dates constrain the diabase to  
 369 have been emplaced between  $1091.83 \pm 0.21$  and  $1091.61 \pm 0.14$  Ma (Figure 6). This  
 370 tight age bracket on the diabase is indistinguishable from the  $1091.59 \pm 0.27$  Ma  $^{206}\text{Pb}/^{238}\text{U}$   
 371 date for the Greenstone Flow of the Portage Lake Volcanics (Fig. 6) — consistent with  
 372 them being comagmatic.

### 373 3.3 Thermal history model

374 The consistency of the paleomagnetic directions between the anorthositic xenoliths  
 375 and the host diabase indicate that the anorthosites were heated above the Curie tem-  
 376 perature of titanomagnetite ( $\sim 580^\circ\text{C}$ ) within the Beaver River diabase. To determine  
 377 whether this thermal history is consistent with the geometry of the units and to gain more  
 378 insight into the emplacement history of the xenoliths, we developed a cooling model. In

379 this model, the anorthosite xenoliths are considered to be solid spheres with an initial  
 380 cool temperature embedded in a uniform sheet of diabase magma (Delaney, 1987; Unsworth  
 381 & Duarte, 1979). The modeled thermal histories for various sizes of anorthosite xeno-  
 382 liths are shown in Figure 7. In one end member case, the initial temperature of the anorthosites  
 383 is assumed to be 50 °C. While this temperature is unrealistically low given the anorthosites  
 384 deep crustal source, thermal modeling shows that even a 100-meter anorthosite xeno-  
 385 lith with such low initial temperature would have been heated to the temperature of the  
 386 tholeiitic magma (1150 °C). This temperature is well above the Curie temperature of  
 387 magnetite. Anorthosite xenoliths with an assumed initial temperature of 500 °C will equi-  
 388 librate with the magma temperature on a similar, but slightly shorter, timescale. There-  
 389 fore, the model predicts that the remanent magnetizations of the anorthosites will al-  
 390 ways be reset during emplacement within the diabase sills, regardless of their initial tem-  
 391 peratures. Model parameters set to match the xenolith AX16 leads to a model where  
 392 the 27.5 m xenolith would have stayed at the magma temperature for about 100 years  
 393 after sill emplacement (Fig. 7). This duration estimate is a minimum as it does not con-  
 394 sider heating associated with melt in the lower crust or during ascent prior to emplace-  
 395 ment. The xenolith would have then cooled through the magnetite Curie temperatures  
 396 (580°) after ~1 kyr and acquired its magnetization as it cooled through magnetite block-  
 397 ing temperatures (down to ~500°).

## 398 4 Discussion

### 399 4.1 Origin of the anorthosite xenoliths

400 U-Pb zircon dates nearly always record the timing of crystallization as the tem-  
 401 peratures required for diffusive loss typically exceed the liquidus such that rock would  
 402 melt before zircons are thermally reset. In this context, the new U-Pb zircon date of 1091.83  
 403 ± 0.21 Ma for an anorthosite xenolith in this study would support crystallization of the  
 404 anorthosite cumulates it represents just before Beaver River diabase emplacement. How-  
 405 ever, the melting point of anhydrous plagioclase with an average composition of the Beaver  
 406 River anorthosite (~70% anorthite, Morrison et al. (1983); Doyle (2016)) is ~1400°C which  
 407 is well above the temperature of the olivine tholeiitic magma in which the xenoliths were  
 408 entrained (~1150 to 1250°C). As a result, zircon U-Pb system in the anorthosites could  
 409 have remained open after the anorthosites crystallized (Fig. 7). The recrystallization tex-  
 410 ture of the anorthosites, as well as the thermal modeling, indicate that the anorthosite

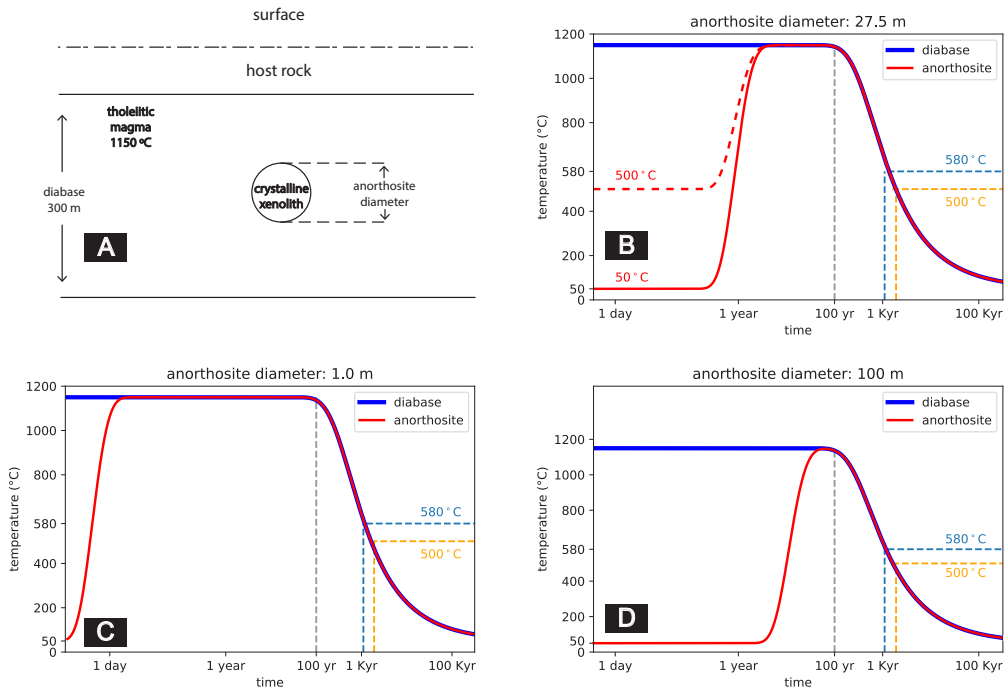


**Figure 7.** Thermal history model of the Beaver River diabase and its anorthosite xenoliths after emplacement at hypabyssal depths. (A) Schematic diagram for the thermal model considering cool anorthosite xenoliths as crystalline spheres residing in the middle of a hot diabase melt. Together they are hosted by cool country rocks at shallow depths. (B) Specific model for anorthosite AX16. Its diameter is measured in field to be 27.5 meters, its diabase sill containing it is estimated to be 323 meters thick. (C) Thermal history model considering an anorthosite xenolith 1 meter in diameter residing in a 300 meter diabase sill. (D) Thermal history model considering an anorthosite xenolith 100 meter in diameter residing in a 300 meter diabase sill. These models show that anorthosite xenoliths were heated up to the diabase melt temperature after the emplacement, regardless of size. The time elapsed between at magnetite blocking temperatures (580 °C and 500 °C) during cooling is on the scale of a thousand years.

xenoliths were indeed heated to elevated temperatures during their emplacement within the diabase. The duration of this heating is difficult to constrain as the anorthosite cumulates could have been heated by mantle-derived magma prior to their liberation and emplacement at shallow depths (it is the final cooling of the sills following magma emplacement that is represented by the thermal modeling; Fig. 7). The magnitude of diffusive Pb loss in crystalline zircon that would (partially) reset the ages is a function of time and temperature (Cherniak & Watson, 2001). For a 100  $\mu\text{m}$  zircon, 100 years at 1150°C (as is modeled for the dated anorthosite xenolith upon emplacement; Fig. 7) would result in 5% Pb loss (Cherniak & Watson, 2001). 100 kyr at this elevated temperature would result in 90% Pb loss (Cherniak & Watson, 2001). As a result, we cannot rule out that the U-Pb date of the anorthosite xenolith has been partially reset. Nevertheless, the crystallization ages of the anorthosite zircons are unlikely to be Paleoproterozoic or Archean (as hypothesized by Morrison et al. (1983)), since that would require nearly all of the Pb to be lost from the zircons to result in a *ca.* 1092 Ma date. Additionally, variable Pb loss between zircons of differing shapes and sizes would lead to discrepant dates between individual grains. These difference would be accentuated for Paleoproterozoic or Archean initial crystallization dates. In contrast, there is tight consistency between the individual zircon dates (Fig. 6) which supports a Midcontinent Rift age albeit one that could be biased young through diffusive loss. As a result, a variety of anorthosite formation scenarios within the Midcontinent Rift system could be compatible with the U-Pb zircon geochronology.

Overall, the origin of anorthositic rocks within the Duluth Complex and the Beaver Bay complexes is likely due to the flotation of plagioclase in lower crustal magma chambers (Fig. 9). As observed experimentally (Kushiro, 1980), the density of plagioclase will be less than that of basaltic magma at pressures of the lower crust. In the *ca.* 1096 Ma Duluth Complex, the flotation of plagioclase caused by this density difference could have created the plagioclase crystal mushes that would have then been extracted and emplaced into the Midcontinent Rift volcanic pile, forming the anorthositic gabbros of the anorthositic series (Fig. 9, Miller and Weiblen (1990); Paces and Miller (1993)). Both the crystal-rich magma that formed the Duluth Complex anorthositic series and more crystal-poor magmas of the Duluth Complex layered series were rapidly emplaced between 1096.19  $\pm$  0.19 Ma and 1095.69  $\pm$  0.18 Ma (Swanson-Hysell et al., 2020). One scenario for the anorthosite xenoliths within the Beaver River diabase is that they formed during this

444 period of Duluth Complex magmatic activity and were subsequently liberated during the  
 445 formation of the Beaver River diabase. The anorthosite xenoliths in the Beaver River  
 446 diabase are coarser and more plagioclase-rich than the anorthositic gabbros of the Du-  
 447 luth Complex such that they are not xenoliths of the Duluth Complex. Additionally, the  
 448 anorthosite xenoliths have higher structural disorder than the Duluth Complex plagi-  
 449 clase which implies that they formed at higher pressure and thereby in a distinct set-  
 450 ting (Miller & Chandler, 1997). A formation age at the time of the Duluth Complex would  
 451 require that repeated ponding of hot ( $>1150^{\circ}\text{C}$ ), mantle-derived magma in the lower crust,  
 452 as well as heating during entrainment within the Beaver River diabase magma, reset-  
 453 ting the U-Pb dates of the xenolith zircons. Alternatively, the anorthosite cumulates rep-  
 454 resented in the xenoliths could have formed just prior to their entrainment in Beaver River  
 455 diabase magma with the U-Pb date being a crystallization age. However, the composi-  
 456 tions of the North Shore Volcanic Group becoming increasingly primitive (Green, 1983)  
 457 and the Portage Lake Volcanics having relatively primitive compositions (Nicholson et  
 458 al., 1997) could support reduced crustal residence times. These data could be interpreted  
 459 as evidence for the waning influence of a fractionally crystallizing, anorthosite-generating,  
 460 deep-crustal magma chamber at the time of the Beaver Bay Complex relative to the Du-  
 461 luth Complex.

462 Regardless of being a crystallization date at the time of anorthosite formation, a  
 463 date modified by (partial) thermal resetting or forming from interstitial melt well after  
 464 plagioclase formation, the U-Pb date of  $1091.83 \pm 0.21$  Ma for the anorthosite xenolith  
 465 constrains the Beaver River diabase to have been emplaced after that date and before  
 466 the  $1091.61 \pm 0.14$  Ma date of the cross-cutting Silver Bay intrusions (Figure 6).

## 467 4.2 A comagmatic relationship between the Beaver River diabase and 468 the Greenstone Flow

469 Given the existence of many anorthosite xenoliths whose short-axis diameters of-  
 470 ten reach tens of meters and can exceed 100 meters (Fig. 1, Boerboom (2004); Boerboom  
 471 et al. (2006)), the Beaver River diabase magma conduits must have been at least this  
 472 wide during magma ascent. It would be consistent with such wide conduits extending  
 473 to hypabyssal depths for magma that flowed through these conduits to have vented to  
 474 the surface. Miller and Chandler (1997) argued that the Portage Lake Volcanics could  
 475 be the surface expression of the Beaver River diabase as they share similar trace element

476 compositions with the diabase and their seismic profile can be correlated with that of  
477 the diabase. This evidence would suggest a cogenetic relationship between the Beaver  
478 River diabase and the Portage Lake Volcanics.

479 Furthermore, the high volume and composite nature of the extrusive Greenstone  
480 Flow of the Portage Lake Volcanics lead to a search for a large and composite feeder sys-  
481 tem. Doyle (2016) proposed a comagmatic link between the Beaver River diabase and  
482 the Greenstone Flow. Doyle (2016) discovered that both the intrusive diabase and the  
483 extrusive volcanics have almost indistinguishable primary compositions that followed sim-  
484 ilar differentiation patterns. Doyle (2016) also points to a shared petrographic textures  
485 between the ophitic Beaver River diabase and the ophitic Greenstone Flow, which fea-  
486 tures the plagioclase laths clustering together and joining along their long crystallographic  
487 axes. The fosterite content of the olivines and enstatite content of the pyroxenes in the  
488 Beaver River diabase and the Greenstone Flow have overlapping compositions consis-  
489 tent with the same magma (Fig. 8). The composition of the plagioclase within the units  
490 further strengthens this interpretation. Although there is no known large xenoliths in  
491 the Greenstone Flow, plagioclase megacrysts occur in the lava. Analyses of the anorthite  
492 content from plagioclase megacrysts show very similar values between the Beaver River  
493 diabase and the Greenstone Flow basalt (Fig. 8, Doyle (2016)). In both units, the pla-  
494 gioclase cores are more enriched in anorthite than the rim and the groundmass. These  
495 data provide evidence that the core of the plagioclase megacrysts in the Greenstone Flow  
496 derived from a similar source with those in the Beaver River diabase and that the rims  
497 are later overgrowths. These mineralogical similarities are consistent with the interpre-  
498 tation that the Beaver River diabase and the Greenstone Flow have the same magma  
499 source.

500 The hypothesized magmatic linkage between the Beaver River diabase and the Green-  
501 stone Flow can be evaluated using the paleomagnetic pole positions and radiometric dates  
502 from both units (Fig. 5, 6). The heat diffusion model of the cooling history of the anorthositic  
503 xenoliths within the diabase suggest that the time it takes to cool the diabase and anorthositic  
504 from low-Ti titanomagnetite Curie temperature ( $\sim 580^\circ\text{C}$ ) to the blocking temperature  
505 of titanomagnetite grains ( $\sim 500^\circ\text{C}$ ) is about a few thousand years (Fig. 7). This time  
506 scale is close to the typical  $10^4$  years which is considered to be sufficient for averaging  
507 out secular variations of the geomagnetic field. Fig. 5 shows the site mean paleomag-  
508 netic pole positions from all diabase and anorthositic sites in this study against the pre-

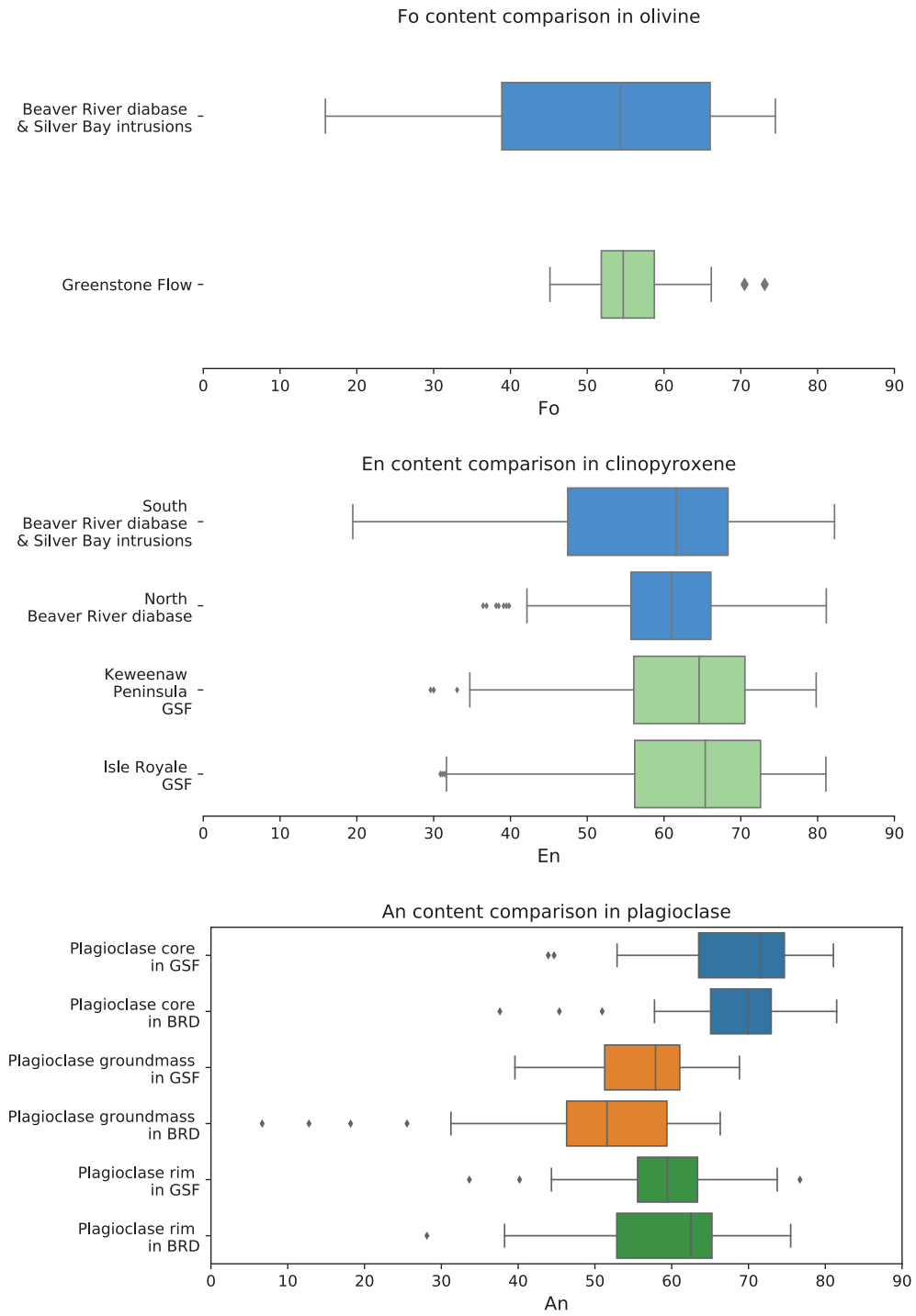


**Figure 8.** Box plots of geochemical analyses of olivine, pyroxene, and plagioclase in the Beaver River diabase (BRD) and Greenstone Flow (GSF). The fosterite content in olivine crystals and the enstatite content in clinopyroxene crystals are very similar in the Beaver River diabase and the Greenstone Flow. The anorthite concentrations in the core, groundmass, and rim of the plagioclase megacrysts within the Beaver River diabase and the Greenstone Flow share very similar patterns and the distributions are nearly identical. Fo-fosterite; En-enstatite; An-anorthite. Data from Doyle (2016).

509 viously synthesized Laurentia APWP developed using an Euler pole inversion to chronos-  
 510 stratigraphically constrained volcanic poles in present-day coordinates (Swanson-Hysell  
 511 et al., 2019). The site-mean pole positions of the diabase and anorthosite overlap within  
 512 uncertainty ellipses and the mean pole positions fall between the 1095 Ma and 1090 Ma  
 513 pole path positions (Fig. 5). Further, the mean paleomagnetic pole position derived from  
 514 the Greenstone Flow share a common mean with those of the Beaver River diabase and  
 515 the anorthosite xenoliths (Fig. 5, Foucher (2018); McFadden and McElhinny (1990), Sup-  
 516 porting Information).

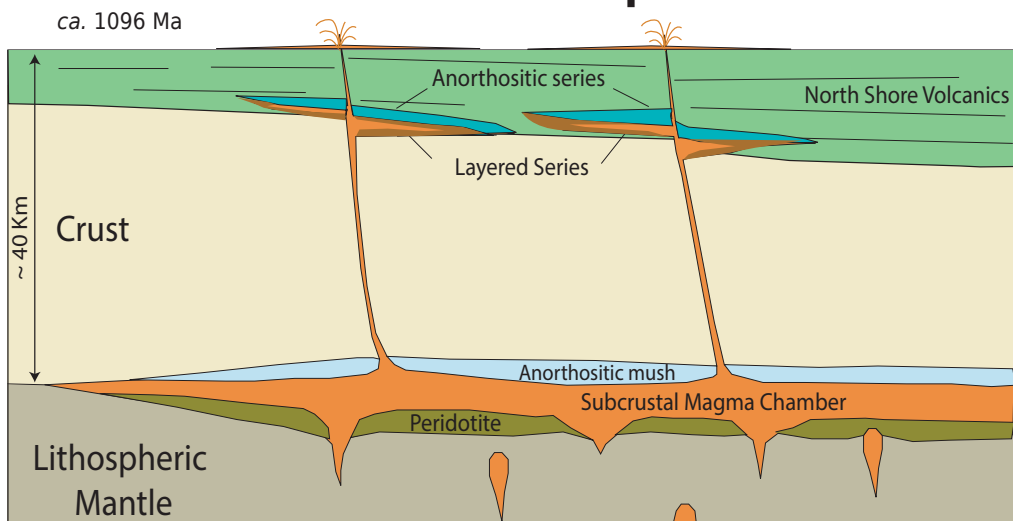
517 Geochronology data agree with the temporal associations revealed by the overlap-  
 518 ping paleomagnetic pole positions. The age of the Beaver River diabase is constrained  
 519 to be between  $1091.83 \pm 0.21$  Ma and  $1091.61 \pm 0.14$  Ma (Fig. 6). This age is indistin-  
 520 guishable with the  $1091.59 \pm 0.27$  Ma age of the Greenstone Flow (Fig. 6). These chrono-  
 521 logical constraints are consistent with a comagmatic linkage between the intrusive Beaver  
 522 River diabase and the extrusive Greenstone Flow.

523 The Portage Lake Volcanics, including the Greenstone Flow, are interpreted to have  
 524 erupted into the main central graben of the Midcontinent Rift during an interval of sig-  
 525 nificant subsidence (Fig. 9, Miller and Chandler (1997); Cannon and Hinze (1992)). In  
 526 contrast to the thick accumulation in the Portage Lake Volcanics, the Beaver Bay Com-  
 527 plex has an erosional (and slightly angular) unconformity atop it that is then covered  
 528 by the the younger Schroeder-Lutsen basalt (Fig. 1, 9, Miller et al. (2001)). This rela-  
 529 tionship suggests that the Beaver River diabase was emplaced into a rift flank highland  
 530 that experienced uplift during the active development of the central graben (Swanson-  
 531 Hysell et al., 2019). Eruptions fed through the Beaver River diabase network could have  
 532 emerged from the rift flank or flowed from the highland into main rift basin where it ac-  
 533 cumulated as the Greenstone Flow (Fig. 9. If the Greenstone Flow indeed connects through  
 534 the Lake Superior basin to NE Minnesota and the Beaver River diabase, the volume of  
 535  $\sim 1650$  km<sup>3</sup> estimated by Longo (1984) must be a minimum.

## 536 5 Conclusion

537 High-precision U-Pb dates, together with paleomagnetic data, support the hypoth-  
 538 esis that the Beaver River diabase was a feeder system to the high-volume Greenstone  
 539 Flow. This intrusive-extrusive linkage is further bolstered by the similar compositions

## Duluth Complex



## Beaver Bay Complex

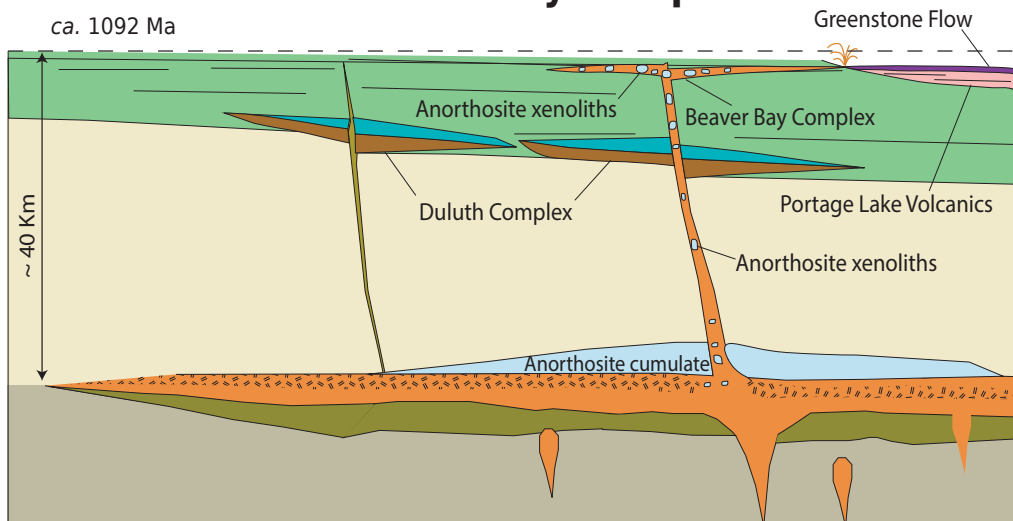


**Figure 9.** Schematic diagrams for the emplacement of the *ca.* 1096 Ma Duluth Complex and the *ca.* 1092 Ma Beaver Bay Complex. The erosional unconformity between the Schroeder-Lutsen basalt and the Beaver River diabase suggest that the Beaver River diabase was emplaced into an uplifted rift flank highland, allowing for flank eruptions of the Greenstone Flow and other Portage Lake Volcanics into the main Midcontinent Rift basin. The total volume of the Greenstone Flow could well exceed the current estimate based on the mapped lava flows on Isle Royale and Keweenaw Peninsula.

540 of the units. The large anorthosite xenoliths require that conduits feeding the magma  
 541 to the surface had diameters that exceeded 150 meters. As a result, there was volumi-  
 542 nous emplacement of magma into the shallow subsurface and erupted into the Midcon-  
 543 tinent Rift basin *ca.* 1092.6 Ma at the end of the main stage of Midcontinent Rift mag-  
 544 matism.

#### 545 Acknowledgments

546 This research was funded by NSF EAR-1847277 to N.L.S.-H. and an Institute on Lake  
 547 Superior Geology Student Research Fund grant to Y.Z. Permits for fieldwork and sam-  
 548 pling from the Minnesota Department of Natural Resources are gratefully acknowledged.  
 549 We thank Stephen Self for providing constructive comments to our manuscript. We thank  
 550 John Grimsich and Tim Teague at UC Berkeley EPS department for their help with pet-  
 551 rographic sample preparation and analyses. Paleomagnetic data associated with this study  
 552 are available within the MagIC database (<https://earthref.org/MagIC/17089/26d9073f-2447-4f46-85fb-8596ce5b3aab>) and all data are within a Github repository associ-  
 553 ated with this work ([https://github.com/Swanson-Hysell-Group/2021\\_AX\\_BD](https://github.com/Swanson-Hysell-Group/2021_AX_BD)) that  
 554 is also archived on Zenodo (insert URL after revisions). This repository also contains  
 555 Python code related to calculations, visualizations and statistical tests discussed herein.  
 556

#### 557 References

- 558 Beck, M. E. (1970). Paleomagnetism of Keweenawan Intrusive Rocks, Min-  
 559 nesota. *Journal of Geophysical Research*, 75(26), 4985–4996. doi:  
 560 [10.1029/jb075i026p04985](https://doi.org/10.1029/jb075i026p04985)
- 561 Beck, M. E., & Lindsley, N. C. (1969). Paleomagnetism of the Beaver Bay Complex,  
 562 Minnesota. *Journal of Geophysical Research*, 74(8), 2002–2013. doi: [10.1029/jb074i008p02002](https://doi.org/10.1029/jb074i008p02002)
- 563 Boerboom, T. J. (2004). *M-147 Bedrock geology of the Split Rock Point quadrangle,*  
*Lake County, Minnesota* (Tech. Rep.). Minnesota Geological Survey.
- 564 Boerboom, T. J., Green, J., & Albers, P. (2007). *M-174 Bedrock geology of the Lut-*  
*sen quadrangle, Cook County, Minnesota* (Tech. Rep.). Minnesota Geological  
 568 Survey.
- 569 Boerboom, T. J., & Green, J. C. (2006). *M-170 Bedrock geology of the Schroeder*  
*quadrangle, Cook County, Minnesota* (Tech. Rep.). Minnesota Geological Sur-

**Table 1.** Summary of new site level paleomagnetic data for the Beaver River diabase and anorthosite xenoliths. n/N: number of samples/sites analyzed and included in the site/grand mean;  $dec_{is}$  &  $inc_{is}$ : in situ mean declination and inclination for the site;  $dec_{tc}$  &  $inc_{tc}$ : tilt-corrected mean declination and inclination for the site; k: Fisher precision parameter; R: resultant vector length;  $\alpha_{95}$ : 95% confidence limit in degrees; VGP lat—latitude of the virtual geomagnetic pole for the site; VGP lon—longitude of the virtual geomagnetic pole for the site. Full measurement level data are available within the MagIC database. <https://earthref.org/MagIC/17102/400e0fb3-a79b-42bd-aeab-9005d2e3b438>.

site	lat	lon	n/N	dec_is	inc_is	dec_tc	inc_tc	k	$\alpha_{95}$	VGP lat_is	VGP lon_is	VGP lat_tc	VGP lon_tc
AX1	47.2	-91.4	8.0	293.3	42.6	288.8	54.9	536.0	2.4	33.4	180.0	37.1	193.2
AX2	47.2	-91.4	9.0	282.0	31.3	277.2	42.6	145.0	4.3	20.4	181.8	22.6	191.1
AX3	47.6	-90.9	10.0	290.4	28.2	285.1	38.6	69.0	5.9	24.7	174.5	25.9	183.7
AX4	47.6	-90.9	7.0	291.9	20.0	288.3	30.7	91.0	6.4	22.3	169.8	24.4	177.2
AX5-10	47.6	-90.9	14.0	286.2	29.1	280.7	38.1	269.5	2.5	22.3	178.1	22.7	186.5
AX11	47.4	-91.2	8.0	284.9	23.5	281.7	35.2	305.0	3.2	19.1	176.3	22.0	184.1
AX12	47.3	-91.3	6.0	299.9	42.5	297.3	55.2	36.0	11.3	37.8	175.1	43.0	188.4
AX13	47.4	-91.2	9.0	289.8	23.0	287.3	35.1	434.0	2.5	22.2	172.4	25.7	180.0
AX14	47.3	-91.3	7.0	296.9	38.2	293.9	50.8	256.0	3.8	33.7	174.5	38.2	186.1
AX15	47.3	-91.3	8.0	282.9	42.3	275.8	53.5	86.0	6.0	26.2	187.2	27.9	199.8
AX16	47.3	-91.3	8.0	273.7	39.1	265.8	49.2	306.0	2.8	18.5	191.6	19.0	202.9
AX17	47.3	-91.3	8.0	273.6	49.8	261.6	59.6	647.0	2.2	24.3	198.3	23.7	213.5
AX18	47.3	-91.3	9.0	283.8	45.5	276.0	56.9	535.0	2.2	28.5	188.7	30.2	202.8
AX19	47.3	-91.3	8.0	293.9	35.8	290.7	48.2	695.0	2.1	30.5	175.4	34.6	186.0
AX20	47.3	-91.3	5.0	294.5	44.3	290.0	56.7	271.0	4.7	35.1	180.4	39.0	194.5
AX21	47.3	-91.3	8.0	301.7	37.7	299.9	50.5	803.0	2.0	36.7	170.4	42.1	181.7
AX22	47.4	-91.2	9.0	297.2	43.1	293.8	55.7	208.0	3.6	36.3	177.6	41.0	191.1
Anorthosite mean		17.0	289.3	36.5	284.5	48.2	55.0	4.9	28.0	179.6	30.9	190.8	
BD1	47.2	-91.4	15.0	293.1	40.9	288.8	53.2	623.0	1.5	32.4	179.0	36.1	191.6
BD2	47.6	-90.9	8.0	286.6	22.7	282.0	32.6	122.0	5.0	19.9	175.0	21.0	182.8
BD3	47.4	-91.2	8.0	286.6	29.8	282.8	41.6	212.0	3.8	22.9	177.9	25.8	186.9
BD4	47.3	-91.3	8.0	300.2	40.7	297.9	53.4	47.0	3.2	37.3	173.6	42.3	186.0
BD5	47.3	-91.3	8.0	282.7	44.8	274.8	56.0	271.0	3.4	27.4	188.9	28.9	202.6
BD6	47.3	-91.3	9.0	300.0	33.2	298.3	46.0	64.0	6.5	33.4	169.2	38.6	178.9
BD7	47.3	-91.3	7.0	292.4	53.1	285.0	65.3	305.0	3.5	38.5	189.2	41.3	208.3
BD8	47.2	-91.4	10.0	287.9	52.8	278.8	64.5	300.0	2.8	35.3	191.8	37.1	209.9
BD9	47.2	-91.3	7.0	278.2	33.8	272.3	44.6	55.0	8.2	19.0	185.7	20.4	195.6
BD10	47.4	-91.2	10.0	297.0	46.2	293.0	58.7	341.0	2.6	37.8	180.0	42.2	195.1
BD11	47.4	-91.3	8.0	296.4	41.7	293.0	54.2	429.0	2.7	35.1	177.1	39.5	189.9
BD12	47.3	-91.3	8.0	288.8	38.1	284.1	50.1	141.0	4.7	28.1	180.4	31.3	191.8
BD13	47.5	-91.1	8.0	280.4	22.4	276.9	33.6	341.0	3.0	15.6	179.2	18.0	186.7
BD15	47.7	-90.6	8.0	300.1	2.3	299.3	14.2	119.0	5.1	20.6	156.9	24.8	161.7
BD17	47.4	-91.2	8.0	295.1	28.5	292.9	41.0	550.0	2.4	28.0	170.8	32.3	179.3
Diabase mean		15.0	291.0	35.7	286.9	47.7	51.6	5.0	29.0	178.2	32.5	189.5	

- 571 vey.
- 572 Boerboom, T. J., Green, J. C., Albers, P., & Miller, J., J.D. (2006). *M-171 bedrock*  
 573 *geology of the tofte quadrangle, cook county, minnesota* (Tech. Rep.). Minnesota  
 574 Geological Survey.
- 575 Books, K. G., White, W. S., & Beck, M. E. (1966). *Magnetization of Keweenawan*  
 576 *gabbro in northern Wisconsin and its relation to time of intrusion.* Geological  
 577 Survey Research.
- 578 Bryan, S. E., Peate, I. U., Peate, D. W., Self, S., Jerram, D. A., Mawby, M. R., ...  
 579 Miller, J. A. (2010). The largest volcanic eruptions on Earth. *Earth-Science*  
 580 *Reviews*, 102(3-4), 207–229. doi: 10.1016/j.earscirev.2010.07.001
- 581 Cannon, W. F., & Hinze, W. J. (1992, oct). Speculations on the origin of the north  
 582 american midcontinent rift. *Tectonophysics*, 213(1-2), 49–55. Retrieved from
- 583 Cherniak, D., & Watson, E. (2001). Pb diffusion in zircon. *Chemical Geology*, 172(1-  
 584 2), 5–24. doi: 10.1016/s0009-2541(00)00233-3
- 585 Condon, D. J., Schoene, B., McLean, N. M., Bowring, S. A., & Parrish, R. R. (2015,  
 586 9 1). Metrology and traceability of U-Pb isotope dilution geochronology  
 587 (EARTHTIME tracer calibration part I). *Geochimica et Cosmochimica Acta*,  
 588 164, 464–480. doi: 10.1016/j.gca.2015.05.026
- 589 Davis, D. W., & Green, J. C. (1997). Geochronology of the North American  
 590 Midcontinent rift in western Lake Superior and implications for its geody-  
 591 namic evolution. *Canadian Journal of Earth Sciences*, 34(4), 476–488. doi:  
 592 10.1139/e17-039
- 593 Davis, D. W., & Paces, J. B. (1990). Time resolution of geologic events on the  
 594 Keweenaw Peninsula and implications for development of the Midcontinent  
 595 Rift system. *Earth and Planetary Science Letters*, 97(1-2), 54–64. doi:  
 596 10.1016/0012-821x(90)90098-i
- 597 Delaney, P. (1987). *Heat transfer during emplacement and cooling of mafic dykes.*  
 598 Geological Association of Canada.
- 599 Doyle, M. (2016). *Geologic and geochemical attributes of the Beaver River Diabase*  
 600 *and Greenstone Flow: Testing a possible intrusive-volcanic link in the 1.1 Ga*  
 601 *Midcontinent Rift* (Unpublished master's thesis). University of Minnesota.
- 602 Fairchild, L. M., Swanson-Hysell, N. L., Ramezani, J., Sprain, C. J., & Bowring,  
 603 S. A. (2017). The end of Midcontinent Rift magmatism and the paleogeogra-

- phy of Laurentia. *Lithosphere*, 9(1), 117–133. doi: 10.1130/l1580.1
- Foucher, M. (2018). *Probing the Precambrian geodynamo: analysis of the geomagnetic field behavior and calibration of pseudo-thellier paleointensity method for Mesoproterozoic rocks* (Unpublished doctoral dissertation). Michigan Technological University.
- Green, J. (1983). Geologic and geochemical evidence for the nature and development of the Middle Proterozoic (Keweenawan) Midcontinent Rift of North America. *Tectonophysics*, 94, 413-437. doi: 10.1016/0040-1951(83)90027-6
- Grout, S. G. M., Frank F. (1939). The geology of the anorthosites of the Minnesota coast of Lake Superior. Minnesota Geological Survey.
- Hinze, W. J., & Chandler, V. W. (2020). Reviewing the configuration and extent of the Midcontinent Rift system. *Precambrian Research*, 342, 105688. doi: 10.1016/j.precamres.2020.105688
- Huber, N. (1973). *The Portage Lake Volcanics (Middle Keweenawan) on Isle Royale, Michigan* (Tech. Rep.). United States Geological Survey.
- Jirsa, M. A., Boerboom, T., Chandler, V., Mossler, J., Runkel, A., & Setterholm, D. (2011). *S-21 Geologic map of Minnesota-bedrock geology* (Tech. Rep.). Minnesota Geological Survey.
- Kushiro, I. (1980). Viscosity, density, and structure of silicate melts at high pressures, and their petrological applications. *Physics of magmatic processes*, 93-120.
- Lane, A. C. (1911). The Keweenaw series of Michigan. *Michigan Geological and Biological Survey Publication 6*, 2(4), 983.
- Lawson, A. C. (1893). The anorthosites of the Minnesota Coast of Lake Superior: Geological and Natural History Survey of Minnesota. *Bulletin*, 8, 1-23.
- Longo, A. A. (1984). *A correlation for a middle Keweenawan flood basalt: the Greenstone flow, Isle Royale and Keweenaw Peninsula, Michigan* (Unpublished master's thesis). Michigan Technological University.
- Mattinson, J. M. (2005). Zircon U-Pb chemical abrasion (“CA-TIMS”) method: Combined annealing and multi-step partial dissolution analysis for improved precision and accuracy of zircon ages. *Chemical Geology*, 220(1-2), 47–66. doi: 10.1016/j.chemgeo.2005.03.011
- McFadden, P., & McElhinny, M. (1990). Classification of the reversal test in palaeo-

- 637 magnetism. *Geophysical Journal International*, 103, 725–729.
- 638 Miller, J., J.D. (1988). *M-065 Geologic map of the Silver Bay and Split Rock Point*  
639 *NE quadrangles, Lake County, Minnesota* (Tech. Rep.).
- 640 Miller, J., J.D., & Boerboom, T. J. (1989). *M-066 geologic map of the Illgen City*  
641 *quadrangle, Lake County, Minnesota* (Tech. Rep.). Minnesota Geological Sur-  
642 vey.
- 643 Miller, J., J.D., & Chandler, V. W. (1997). Geology, petrology, and tectonic signifi-  
644 cance of the Beaver Bay Complex, northeastern Minnesota. In *Middle Protero-*  
645 *zoic to Cambrian rifting, central North America*. Geological Society of Amer-  
646 ica. doi: 10.1130/0-8137-2312-4.73
- 647 Miller, J., J.D., & Ripley, E. (1996). Layered Intrusions of the Duluth Complex,  
648 Minnesota, USA. *Layered Intrusions*, 257–301. doi: 10.1016/s0167-2894(96)  
649 80010-8
- 650 Miller, J., J.D., Severson, M. J., Chandler, V. W., & Peterson, D. M. (2001). *M-119*  
651 *Geologic map of the Duluth Complex and related rocks, northeastern Minnesota*  
652 (Tech. Rep.). Minnesota Geological Survey.
- 653 Miller, J., J.D., & Weiblen, P. W. (1990). Anorthositic rocks of the Duluth Com-  
654 plex: Examples of rocks formed from plagioclase crystal mush. *Journal of*  
655 *Petrology*, 31(2), 295–339. doi: 10.1093/petrology/31.2.295
- 656 Morrison, D. A., Ashwal, L. D., Phinney, W. C., Shih, C.-Y., & Wooden, J. L.  
657 (1983). Pre-Keweenawan anorthosite inclusions in the Keweenawan Beaver Bay  
658 and Duluth Complexes, northeastern Minnesota. *Geological Society of America*  
659 *Bulletin*, 94(2), 206. doi: 10.1130/0016-7606(1983)94<206:paiitk>2.0.co;2
- 660 Nicholson, S. W., Schulz, K. J., Shirey, S. B., & Green, J. C. (1997). Rift-wide  
661 correlation of 1.1Ga Midcontinent rift system basalts: implications for multiple  
662 mantle sources during rift development. *Canadian Journal of Earth Sciences*,  
663 34(4), 504–520. doi: 10.1139/e17-041
- 664 Paces, J. B., & Miller, J., J.D. (1993). Precise U-Pb ages of Duluth Complex and  
665 related mafic intrusions, northeastern Minnesota: Geochronological insights  
666 to physical, petrogenetic, paleomagnetic, and tectonomagmatic processes as-  
667 sociated with the 1.1 Ga Midcontinent Rift System. *Journal of Geophysical*  
668 *Research: Solid Earth*, 98(B8), 13997–14013. doi: 10.1029/93jb01159
- 669 Self, S., Jay, A., Widdowson, M., & Keszthelyi, L. (2008). Correlation of the Deccan

- 670 and Rajahmundry Trap lavas: Are these the longest and largest lava flows on  
671 Earth? *Journal of Volcanology and Geothermal Research*, 172(1-2), 3–19. doi:  
672 10.1016/j.jvolgeores.2006.11.012
- 673 Swanson-Hysell, N. L., Hoaglund, S. A., Crowley, J. L., Schmitz, M. D., Zhang,  
674 Y., & Miller, J. D. (2020). Rapid emplacement of massive Duluth Com-  
675 plex intrusions within the North American Midcontinent Rift. *Geology*. doi:  
676 10.1130/g47873.1
- 677 Swanson-Hysell, N. L., Maloof, A. C., Weiss, B. P., & Evans, D. A. D. (2009).  
678 No asymmetry in geomagnetic reversals recorded by 1.1-billion-year-old ke-  
679 weenawan basalts. *Nature Geoscience*, 2(10), 713–717. Retrieved from doi:  
680 10.1038/ngeo622
- 681 Swanson-Hysell, N. L., Ramezani, J., Fairchild, L. M., & Rose, I. R. (2019). Failed  
682 rifting and fast drifting: Midcontinent Rift development, Laurentia's rapid mo-  
683 tion and the driver of Grenvillian orogenesis. *GSA Bulletin*, 131(5-6), 913–940.  
684 doi: 10.1130/b31944.1
- 685 Tauxe, L., Shaar, R., Jonestrask, L., Swanson-Hysell, N. L., Minnett, R., Koppers,  
686 A. A. P., … Fairchild, L. (2016). PmagPy: Software package for paleomag-  
687 netic data analysis and a bridge to the Magnetics Information Consortium  
688 (MagIC) Database. *Geochemistry, Geophysics, Geosystems*, 17(6), 2450–2463.  
689 doi: 10.1002/2016gc006307
- 690 Unsworth, J., & Duarte, F. J. (1979). Heat diffusion in a solid sphere and Fourier  
691 theory: An elementary practical example. *American Journal of Physics*,  
692 47(11), 981–983. doi: 10.1119/1.11601
- 693 van Hinsbergen, D. J. J., Steinberger, B., Doubrovina, P. V., & Gassmöller, R.  
694 (2011). Acceleration and deceleration of India-Asia convergence since the  
695 Cretaceous: Roles of mantle plumes and continental collision. *Journal of  
696 Geophysical Research*, 116(B6). doi: 10.1029/2010jb008051
- 697 Vervoort, J. D., Wirth, K., Kennedy, B., Sandland, T., & Harpp, K. S. (2007). The  
698 magmatic evolution of the Midcontinent rift: New geochronologic and geo-  
699 chemical evidence from felsic magmatism. *Precambrian Research*, 157(1-4),  
700 235–268. doi: 10.1016/j.precamres.2007.02.019
- 701 White, W. (1960). The Keweenawan lavas of Lake Superior, an example of flood  
702 basalts. *American Journal of Science*, 258, 367–374.